IUST
Iran University of Science and Technology

Iranian Journal of Electrical and Electronic Engineering

Journal Homepage: ijeee.iust.ac.ir

Research Paper

Semi-Analytical Modeling of Electromagnetic Performances in Magnet Segmented Spoke-Type Permanent Magnet Machine Considering Infinite and Finite Soft-Magnetic Material Permeability

A. Jabbari*(C.A.)

Abstract: In this paper, we present a semi-analytical model for determining the magnetic and electromagnetic characteristics of spoke-type permanent magnet (STPM) machine considering magnet segmentation and finite soft-material relative permeability. The proposed model is based on the resolution of the Laplace's and Poisson's equations in a Cartesian pseudo-coordinate system with respect to the relative permeability effect of iron core in a subdomain model. Two different magnet-segmented STPM machine was studied analytically and numerically. The effect of the iron core relative permeability on the STPM machine performances was investigated at no-load and on-load conditions with respect to certain values of iron core relative permeability by comparing cogging torque, electromagnetic torque ripple, and reluctance torque ripple waveforms. In order to validate the results of the proposed analytical model, the analytical and numerical results were compared. It can be seen that the analytical modeling results are consistent with the results of numerical analysis.

Keywords: Semi-Analytical Model, Spoke-Type Permanent Magnet Machine, Magnet Segmentation, Finite Iron Core Relative Permeability, Quasi-Cartesian Coordinates, Subdomain Technique.

1 Introduction

A segmented pole consists of two or more PM pieces located beside each other with a certain gap between each piece. Researchers have identified the spoke-type permanent magnet machine as one of the most suitable machines for high-speed applications as a good alternative to surface mounted PM machines. Magnet segmentation is used as one of the effective methods for reducing pulsating torque components in permanent magnet machines [1-3].

An analytical method that minimizes the cogging torque in rotor surface mounted permanent-magnet motors presented in [2]. The main idea in this work is to set the distribution of the air-gap flux density by segmenting the permanent magnet into several primitive magnet blocks. The analytical approach uses Fourier-Maxwell expansion to estimate the cogging torque harmonics, and finite-element computations.

An accurate analytical model of a double-sided air-core linear permanent-magnet machine with segmented permanent-magnet poles has been presented in [3]. The average thrust as well as thrust ripple was precisely calculated by this model. Back-electromotive force and flux density distribution of the motor are also determined by this method. This model provides the analytical framework for design optimization of double-sided air-core permanent-magnet linear synchronous motors with segmented poles regarding more motor parameters and objectives.

The flux weakening mechanism of interior permanent magnet synchronous machines with segmented

Iranian Journal of Electrical and Electronic Engineering, 2021.
Paper first received 11 November 2019, revised 11 April 2020, and accepted 22 April 2020.
* The author is with the Mechanical Engineering Department, Arak University, Arak, Iran.
E-mail: jabbari@araku.ac.ir.
Corresponding Author: A. Jabbari.
https://doi.org/10.22068/IJEEE.17.1.1711

permanent magnets (PMs) in the rotor was studied in [4]. Air gap flux density with and without segments are analyzed and compared, based on both analytical and finite element methods. Frozen permeability technique is used to separate the PM component flux density in iron bridges at load condition, to find out the effect of demagnetizing current on flux variation. A novel explanation is proposed to explain the improvement effect of the flux weakening capability by magnet segmentation.

A novel interior permanent magnet machines used for spindle drive where wide constant power speed range is necessary [5]. To obtain wide constant power speed range, segmented permanent magnet was adopted. Besides, in order to check the influences of segmented permanent magnet on cogging torque, it was also analyzed by finite element analysis.

The effect of segmentation on the losses was estimated by a 3-D time-harmonic finite element model for sinusoidal waveforms [6]. It is shown that more segmentation of the magnets in axial and circumferential direction results in much lower losses in the magnets, but more losses in the massive rotor yoke.

In [7], the lumped magnetic circuit models are used for interior permanent magnet (IPM) machines with multi-segment and multilayer permanent magnets. The open-circuit air gap field distribution, average air gap flux density and leakage fluxes are derived analytically.

The impacts of the stator slot with skew and segment magnet rotor on the performance of interior permanent magnet (IPM) machine for an electric traction was studied in [8]. Comparisons of the average torque, torque ripples, cogging torque and no-load back EMF with skew and un-skew are given and how suitable a segmented rotor IPM machine and its torque characteristic and the field weakening capability are investigated. From the FEA results, it shows that the IPM synchronous machine with two-teeth stator slots skewed and two-segmented magnet rotor has better performance than the conventional IPM synchronous machine.

In another work, the effect of eddy current loss reduction by segmented rare-earth magnets that are used in synchronous motors driven by inverters was investigate in [9]. First, the difference in the loss-reduction effect due to the rotor shape is estimated by the 3-D finite-element analysis that considers the carrier harmonics of the inverter. The results are compared to the theoretical solution. Next, a basic experiment using magnet specimens is carried out in order to confirm the calculated results.

The characteristics of the magnetic force acting on the segmented magnets was analyzed and the events they can possibly cause was predicted in [10].

The magnet segmentation effects on eddy current losses in magnets was studied in [11]. A 2D non-linear model based on finite element analysis is developed under MATLAB environment. The developed model is applied to a synchronous machine with surface mounted permanent magnets. An optimization process which consists to associate the finite element analysis to genetic algorithm in order to find the best parameters of magnets segmentation and avoid any segmentations anomaly that appears under some conditions such as skin effect, and which can lead to losses increases instead of their reduction.

To analyze the effect of the gap between segments on air-gap flux density, an analytical model of the Halbach array permanent magnet machine considering the gap between segments is established in [12]. The finite element model is adopted to validate the established analytical model. Furthermore, effects of the parameters of the segmented Halbach array, including gap between segments, segment number per pole, and pole pair number on the fundamental amplitude, and waveform distortion factor of the radial component of air-gap flux density are analyzed using the established analytical model.

In [13], a switched flux permanent magnet (SFPM) machine with radially segmented permanent magnets (PMs) is presented. The thickness of each segment is optimized to maximize the torque performance and reduce the total magnet material volume. The influence of the number of segments is studied by testing a different number of segments. Furthermore, a comparison between a conventional with non-segmented magnets (CSFPM) machine, an SFPM machine with trapezoidal-shaped magnets (TSFPM) and the proposed machine with segmented magnets (SSFPM) is presented. It is found that, the SSFPM has higher torque and higher torque per magnet volume than that of the CSFPM and TSFPM machines.

An analysis of using segmented permanent magnet instead of single pole units on a synchronous generator was presented in [14]. The main reason of using such solutions is the fact that smaller, simple shapes permanent magnets with standardized dimensions can easily be found on the market at low costs.

From the study of the literature survey, it can be concluded that the effect of magnet segmentation on the performance of spoke-type machine has not been investigated so far. Various methods such as numerical, analytical and experimental methods are used to determine the performance characteristics of electric machines. Generally, numerical methods can be used to estimate the magnetic field in STPM machines [15]. Although these methods are highly accurate, their main drawback is that they are time consuming. Therefore, researchers are trying to provide analytical models to accurately calculate the no-load/on-load performance of the electric machines in the initial and optimization stages.

Some reviews of analytical modeling techniques in electrical machines for magnetic field and performance computation were provided in [16-18]. A semi-analytical method for synchronous reluctance motor

analysis including finite soft-magnetic material permeability was presented in [19]. Djelloul *et al*. developed a nonlinear analytical model in order to calculate the magnetic field and electromagnetic performances in switched reluctance machines [20]. Roubache *et al*. provide a new subdomain technique for electromagnetic performance calculation in radial-flux electrical machines considering finite soft-magnetic material permeability [21]. Jabbari presented a Maxwell-Fourier based analytical method in order to calculate magnetic vector potential in surface mounted and surface inset permanent magnet machines in [22] and magnet segmented surface inset PM machines in [23]. The resolution of Laplace's and Poisson's equations was performed in a quasi-Cartesian coordinates system. He also presented an analytical model to estimate the magnetic field distribution in multiphase H-type stator core permanent magnet flux switching machines [24]. An analytical expression for magnet shape optimization in surface-mounted permanent magnet machines and iron pole shape optimization in interior permanent magnet machines was derived in [25] and [26], respectively.

Analytical solution of the no-load vector potential and flux density in permanent-magnet motors taking into account slotting effect was studied in [27]. Dubas *et al*. presented a new scientific contribution on the 2-D subdomain technique in Cartesian coordinates taking into account of iron parts [28]. An analytical computation of magnetic field in parallel double excitation and spoke-type permanent magnet machines accounting for tooth-tips and shape of polar pieces presented in [29]. Liang *et al*. provided an analytical model in order to estimate magnetic field distribution in spoke-type permanent-magnet synchronous machines accounting for bridge saturation and magnet shape [30]. Pourahmadi-Nakhli *et al*. presented an analytical method to model the slotted brushless machines with cubic spoke-type permanent magnets [31]. A new subdomain method for performances computation in interior permanent-magnet (IPM) machines considering iron core relative permeability was presented by Jabbari *et al*. [32].

To the best of the author's knowledge, in no reference, an analytical model has been presented to determine the electromagnetic performances of STPM machine considering magnet segmentation as well as the iron core relative permeability. The proposed model is obtained by solving the Maxwell equations by considering the appropriate boundary conditions in the Cartesian pseudo-coordinate system.

2 Magnet-Segmentation definition in Spoke Type Machine

In Fig. 1, two types of STPM machines are shown, as in type (a), two pieces of magnet with two air-gap regions and in type (b), two pieces of magnet with one air-gap region, both with tangential magnetization orientation are arranged and every combination defines a machine pole. The subdomain model of the investigated machine is shown in Fig. 2 with the region symbols described in Table 1. The machine regions can be defined as periodic or non-periodic regions. In Table 2, the periodic and non-periodic regions and the general PDE equations of each region are derived.

Analytical model in the Cartesian pseudo-coordinate system is formulated by the resolution of the Laplace's and Poisson's equations for determining the magnetic potential as $A = \{0; 0; Az\}$. In the solution of the Maxwell equations, we use the following simplifying

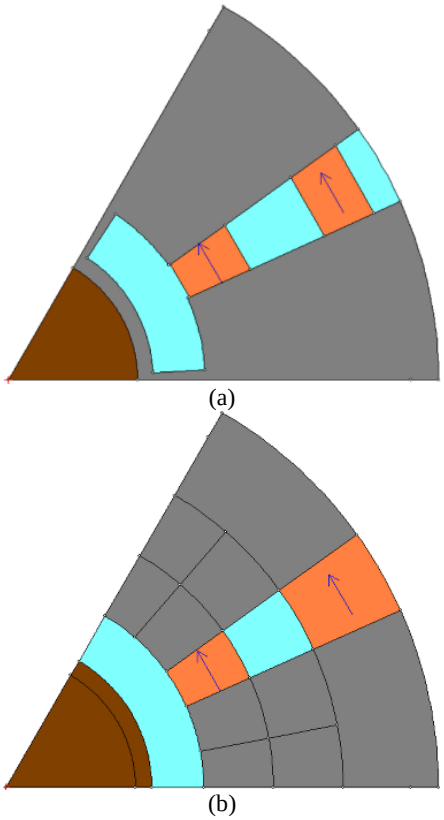

(a) (b)

Fig. 1 Tow studied magnet-segmented STPM machines; a) M1-design with two air-gap and b) M2-design with one air-gap.

Table 1 Representation of the machine regions.

Symbol	Description
Region I	Rotor shaft
Region II	Rotor yoke
Region III	Rotor teeth
Region IV	Rotor slot
Region V	rotor teeth
Region VI	PMs
Region VII	Rotor slot
Region VIII	Rotor teeth
Region IX	Air-gap
Region X and XII	Stator teeth
Region XI	Stator slot-opening
Region XIII	Stator slot (on the left)
Region XIV	Stator slot (on the right)
Region XV	Stator yoke

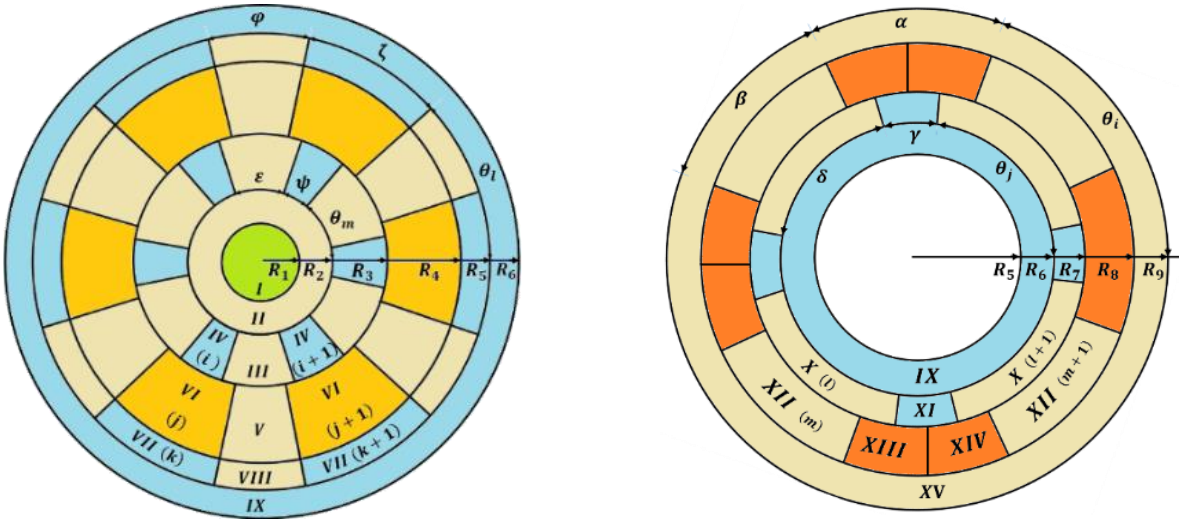

(a) (b)

Fig. 2 The investigated model; a) the rotor subdomains and b) the stator subdomains.

Table 2 Definition of periodic and non-periodic regions and their reprehensive Laplace's or Poisson's equation.

Category	Ω-Region	Laplace's/ Poisson's equation (μ_0 is the vacuum permeability; $\vec{M}$ is the magnetization of the PM; J_z is the current density in the stator slots)	No.
Periodic region	I, II, XI, XV		
Non-periodic region	III, IV, V, VIII, VII, X, XI, XII	$\nabla^2 A_z = \frac{\partial^2 A_\Omega}{\partial t^2} + \frac{\partial^2 A_\Omega}{\partial \theta^2} = 0$	(1)
	VI	$\nabla^2 A_z = -\mu_0 \nabla \times M = \frac{\partial^2 A_{\Omega(g)}}{\partial t^2} + \frac{\partial^2 A_{\Omega(g)}}{\partial \theta^2} = -\mu_0 R_3 e^{-t} M_\theta$	(2)
	XIII and XIIV	$\nabla^2 A_z = -\mu_0 J = \frac{\partial^2 A_\Omega}{\partial t^2} + \frac{\partial^2 A_\Omega}{\partial \theta^2} = -\mu_0 R_7^2 e^{-2t} J_{zi}$	(3)

Table 3 The magnetic material equation for each subdomain.

Region	Equation (μ_{rm} is the relative recoil permeability of PMs and μ_{rc} is the relative recoil permeability of iron parts	No.
I, IV, VII, XI, and XI	$B = \mu_0 H$	(4)
VI	$B = \mu_0 \mu_{rm} H + \mu_0 M$	(5)
II, III, V, VIII, X, XII and XV	$B = \mu_0 \mu_{rc} H$	(6)

assumptions.

1) The axial length of the machine is assumed to be infinitely and the magnetic variables independent of *z*.
2) Stator teeth/slots, the rotor regions have radial sides.
3) The current density, *Jz*, is along the *z*-axis.
4) It is assumed that the electrical conductivity of the material is zero.

Field vectors $B = \{B_t; B_\theta; 0\}$ and $H = \{H_t; H_\theta; 0\}$ are coupled in different regions by means of magnetic material equation as shown in Table 3.

Using $B = \nabla \times A$ the components of B can be deduced by

$$B_t = \frac{e^t}{R_i} \frac{\partial A_z}{\partial \theta} \tag{7}$$

and

$$B_\theta = \frac{e^t}{R_i} \frac{\partial A_z}{\partial t} \tag{8}$$

3 Magnetic Vector Potential Calculation

First, periodic and non-periodic areas are determined in this section, and then the corresponding Laplace's or Poisson's equation is solved by the method of separation of the variables. In order to determine the constants of integration, the boundary conditions and the interface conditions are considered.

The general solution of Laplace's equation for I, II, XI and XV regions by using the separation of variables method and a quasi-Cartesian coordinate system [22] can be described as

$$A_{z\Omega}(t.\theta)=a_0^{\Omega}+b_0^{\Omega}t+\sum_{n=1}^{\infty}\left(a_n^{\Omega}\frac{G_j}{H_{i-j}}+b_n^{\Omega}\frac{G_i}{H_{j-i}}\right)\cos(n\theta)+\sum_{n=1}^{\infty}\left(c_n^{\Omega}\frac{G_j}{H_{i-j}}+d_n^{\Omega}\frac{G_i}{H_{j-i}}\right)\sin(n\theta)$$

$$for\begin{cases}\theta\in[0,2\pi]\\ H_{i-j}=Sh\left(n\left(t_i-t_j\right)\right)\\ H_{j-i}=Sh\left(n\left(t_i-t_j\right)\right)\\ G_j=G\left(n\left(t-t_j\right)\right)\\ G_i=G\left(n\left(t-t_i\right)\right)\end{cases}\quad(9)$$

where n is a positive integer, and

- $G = Sh$, $t \in [t_i = t_1, t_j = t_2]$ and $b_n^{\Omega} = d_n^{\Omega} = 0$ for (Ω = I),
- $G = Sh$, $t \in [t_i = t_3, t_j = t_4]$, for ($\Omega$ = II),
- $G = Sh$, $t \in [t_i = t_{17}, t_j = t_{18}]$ and $bn^{\Omega} = d_n^{\Omega} = 0$ for (Ω = XV),
- $G = Sh$, $t \in [t_i = t_{11}, t_j = t_{12}]$ for (Ω = XI).

By using the separation of variables method, the general solution of Laplace's equation for III, IV, V, VIII, VII, X, XI, and XII regions can be as

$$A_{z\Omega(g)}(t.\theta)=a_0^{\Omega(g)}+b_0^{\Omega(g)}t+\sum_{h=1}^{\infty}\left(\frac{a_h^{\Omega(g)}}{\nu_{h.\Omega(g)}}\frac{G_j}{H_{i-j}}+\frac{b_h^{\Omega(g)}}{\nu_{h.\Omega(g)}}\frac{G_i}{H_{j-i}}\right)\cos\left(\nu_{h.\Omega(g)}(\theta-\theta_1)\right)+\sum_{k=1}^{\infty}\left(\frac{a_k^{\Omega(g)}}{\nu_{k.\Omega(g)}}\frac{H_1}{H_0}+\frac{b_k^{\Omega(g)}}{\nu_{k.\Omega(g)}}\frac{H_2}{H_0}\right)\sin\left(\nu_{k.\Omega(g)}t\right)$$

$$for\begin{cases}\theta\in[\theta_1,\theta_2]\\ \nu_{h.\Omega(g)}=h\pi/\Theta\\ \nu_{k.\Omega(g)}=k\pi/t_j\\ H=Sh\\ H_{i-j}=H\left(\nu_{h.\Omega(g)}\left(t_i-t_j\right)\right)\\ H_{j-i}=H\left(\nu_{h.\Omega(g)}\left(t_j-t_i\right)\right)\\ H_1=H\left(\nu_{k.\Omega(g)}(\theta-\theta_1)\right)\\ H_2=H\left(\nu_{k.\Omega(g)}(\theta-\theta_2)\right)\\ G_i=G\left(\nu_{h.\Omega(g)}\left(t-t_i\right)\right)\\ G_j=G\left(\nu_{h.\Omega(g)}\left(t-t_j\right)\right)\\ H_0=H\left(\nu_{k.\Omega(g)}\Theta\right)\end{cases}\quad(10)$$

where

- $t \in [t_{15}, t_{16}]$, $\Theta = \beta$, $\theta \in [\theta_1, \theta_2] = [\theta_i + \alpha, \theta_i + \alpha + \beta]$, $\Omega(g)$ = XII(m) and $G = Ch$ for m-th stator teeth,
- $t \in [t_{13}, t_{14}]$, $\Theta = \delta$, $\theta \in [\theta_j + \gamma, \theta_j + \gamma + \delta]$, $\Omega(g)$ = X(l) and $F = Ch$ for l-th stator teeth,
- $t \in [t_{13}, t_{14}]$, $\Theta = \gamma$, $\theta \in [\theta_j, \theta_j + \gamma]$, $G = Sh$, $\Omega(g)$ = XI(l) and $a_k^{\Omega(g)} = b_k^{\Omega(g)} = 0$ for l-th stator slot-opening,
- $t \in [t_9, t_{10}]$, $\Theta = \zeta$, $\theta \in [\theta_l, \theta_l + \zeta]$, $a_k^{\Omega(g)} = b_k^{\Omega(g)} = 0$, $G = Sh$ and $\Omega(g)$ = VII(k) for k-th rotor outer slot,
- $t \in [t_9, t_{10}]$, $\Theta = \varphi$, $\theta \in [\theta_l + \zeta, \theta_l + \zeta + \varphi]$, $G = Ch$ and $\Omega(g)$ = VIII(k) for k-th rotor teeth,
- $t \in [t_7, t_8]$, $\Theta = \varphi$, $\theta \in [\theta_l + \zeta, \theta_l + \zeta + \varphi]$, $G = Ch$ and $\Omega(g)$ = V(j) for j-th rotor teeth,
- $t \in [t_5, t_6]$, $\Theta = \psi$, $\theta \in [\theta_m, \theta_m + \psi]$, $a_k^{\Omega(g)} = b_k^{\Omega(g)} = 0$, $G = Sh$ and $\Omega(g)$ = IV(i) for i-th rotor inner slot,
- $t \in [t_5, t_6]$, $\Theta = \varepsilon$, $\theta \in [\theta_m + \psi, \theta_m + \psi + \varepsilon]$, $G = Ch$ and $\Omega(g)$ = III(i) for i-th rotor teeth.

The general solution of Poisson's equation for VI region by using the separation of variables method can be described as

$$A_{z\Omega(g)}(t.\theta)=a_0^{\Omega(g)}+b_0^{\Omega(g)}t-h_{\Omega(g)}(t)+\sum_{h=1}^{\infty}\left(\frac{a_h^{\Omega(g)}}{\nu_{h.\Omega(g)}}\frac{G_j}{H_{i-j}}+\frac{b_h^{\Omega(g)}}{\nu_{h.\Omega(g)}}\frac{G_i}{H_{j-i}}+Y_h^{I}\right)\cos\left(\nu_{h.\Omega(g)}(\theta-\theta_1)\right)+\sum_{k=1}^{\infty}\left(\frac{a_k^{\Omega(g)}}{\nu_{k.\Omega(g)}}\frac{H_1}{H_0}+\frac{b_k^{\Omega(g)}}{\nu_{k.\Omega(g)}}\frac{H_2}{H_0}\right)\sin\left(\nu_{k.\Omega(g)}t\right)$$

$$for\begin{cases}h_{\Omega(g)}(t)=R_3e^{-t}(-1)^i\,B_r(\theta-\theta_1)\\ t\in[t_7,t_8]\\ \theta\in[\theta_1,\theta_2]=[\theta_l,\theta_l+\zeta]\\ Y_h^{I}=X_h^{I}(t)\cos\left(\nu_{h.\Omega(g)}\varphi_i\right)\\ \nu_{h.\Omega(g)}=h\pi/\Theta\\ \nu_{k.\Omega(g)}=k\pi/t_j\\ \Theta=\zeta\\ \Omega(g)=VI(j)\\ H_{i-j}=Sh\left(\nu_{k.\Omega(g)}\left(t_i-t_j\right)\right)\\ H_{j-i}=Sh\left(\nu_{k.\Omega(g)}\left(t_j-t_i\right)\right)\\ H_0=Sh\left(\nu_{k.\Omega(g)}\Theta\right)\\ H_1=Sh\left(\nu_{k.\Omega(g)}(\theta-\theta_1)\right)\\ H_2=Sh\left(\nu_{k.\Omega(g)}(\theta-\theta_2)\right)\\ G_j=Ch\left(\nu_{h.\Omega(g)}\left(t-t_j\right)\right)\\ G_i=Ch\left(\nu_{h.\Omega(g)}\left(t-t_i\right)\right)\end{cases}\quad(11)$$

By using the separation of variables method, the general solution of Poisson's equation XIII and XIIV regions can be as

$$A_{z\Omega(g)}(t.\theta)=a_k^{\Omega(g)}+b_k^{\Omega(g)}t-h_{z\Omega(g)}(t)+\sum_{h=1}^{\infty}\frac{a_k^{\Omega(g)}}{\nu_{h.\Omega(g)}}\frac{G_j}{H_{i-j}}\cos\left(\nu_{h.\Omega(g)}(\theta-\theta_1)\right)+\sum_{k=1}^{\infty}\left(\frac{a_k^{\Omega(g)}}{\nu_{k.\Omega(g)}}\frac{H_1}{H_0}+\frac{b_k^{\Omega(g)}}{\nu_{k.\Omega(g)}}\frac{H_2}{H_0}\right)\sin\left(\nu_{k.\Omega(g)}t\right)$$

$$for\begin{cases}h_{z\Omega(g)}(t)=\frac{1}{4}\mu_0 J_{z\Omega(g)}e^{-2t}\\ \theta\in[\theta_1,\theta_2]\\ t\in\left[t_i,t_j\right]=[t_{15},t_{16}]\\ \Theta=\alpha/2\\ \nu_{h.\Omega(g)}=h\pi/\Theta\\ \nu_{k.\Omega(g)}=k\pi/t_j\\ H_{i-j}=Sh\left(\nu_{h.\Omega(g)}(t_i-t_j)\right)\\ H_0=Sh\left(\nu_{k\Omega(g)}\Theta\right)\\ H_1=Sh\left(\nu_{k.\Omega(g)}(\theta-\theta_1)\right)\\ H_2=Sh\left(\nu_{k.\Omega(g)}(\theta-\theta_2)\right)\\ G_j=Ch\left(\nu_{h.\Omega(g)}(t-t_j)\right)\end{cases}\quad(12)$$

where

- $\theta \in [\theta_i, \theta_i + \alpha/2]$ and $\Omega(g)$ = XIII(m) for m-th stator slot-right *side* and
- $\theta \in [\theta_i + \alpha/2, \theta_i + \alpha]$ and $\Omega(g)$ = XIV(m) for m-th stator slot-left side.

To determine the integration constants in (9)-(12); the boundary conditions at the interface between the different regions should be introduced. In non-homogenous regions, we consider the interface conditions in two edges (i.e., t- and θ–edges) as listed in the Appendix.

4 Results and Evaluation

In order to study the effect of magnet segmentation on performance characteristics of STPM machine, an 8P-18S spoke type machine with two different topologies has been modeled analytically and numerically. The two-dimensional analytical representation for STPMM, considering the magnet segmentation and distinct material permeability is applied to estimate the machine performances. The main dimensions and parameters of the investigated STPMMs are given in Table 4. Fig. 3 shows the rotor geometrical lines, material shade and mesh density distribution of the investigated machines. 2-D geometrical model and magnetic flux density distribution in two investigated machines for infinite relative permeability of iron cores are presented in Fig. 4.

On-load magnetic performance characteristics at the middle of air-gap including radial flux density, tangential flux density, x- and y- components of flux density, Maxwell tensor of torque, Maxwell tensor of normal force, x- and y- components of force for M1 and M2 machines are shown in Fig. 5 and Fig. 6, respectively. It is shown that the analytical results at each certain value are in good agreement with the results of the numerical method with an error percent of about 4.3%.

Electromagnetic performances of the investigated machines at nominal condition including the electromagnetic torque, reluctance torque, phase

Table 4 Parameters of studied machines.

Symbol	Parameters	Value				Unit
		M1		M2		
B_{rm}	Remanence flux density of PMs	1				T
μ_{rm}	Relative permeability of PMs	1				
N_c	Number of conductors per stator slot	120				
I_m	Peak phase current	10				A
Q_s	Number of stator slots	6				
c	Stator slot-opening	30				deg.
a	PM opening	18				deg.
p	Number of pole pairs	3				-
R_4	Outer radius of stator slots	60.3				mm
R_3	Radius of the stator inner surface	45.3				mm
R_2	Radius of the rotor outer surface at the PM surface	44.8				mm
R_1	Radius of the rotor inner surface at the PM bottom	18				mm
g	Air-gap length	0.5				mm
L_u	Axial length	57				mm
n	Mechanical pulse of synchronism	10000				rpm
	Magnet widths	up	down	up	down	mm
		2.86	3.5	5.36	3.5	

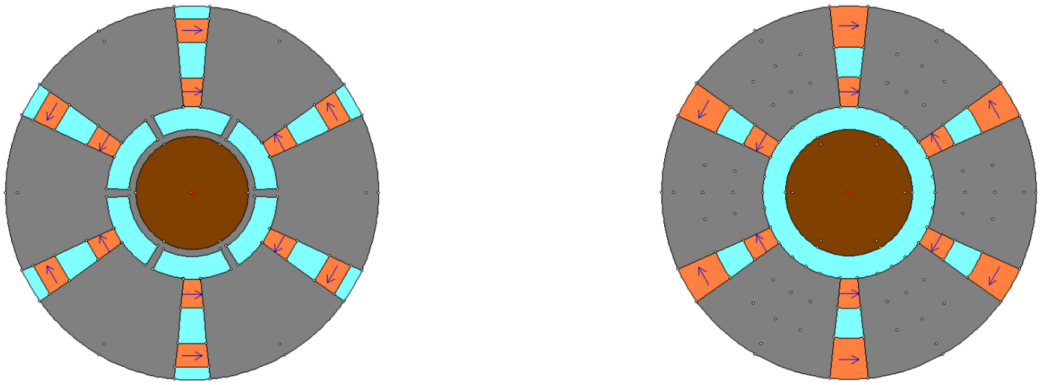

(a) (b)

Fig. 3 The geometry/material shade and mesh density in a) M1-rotor and b) M2-rotor.

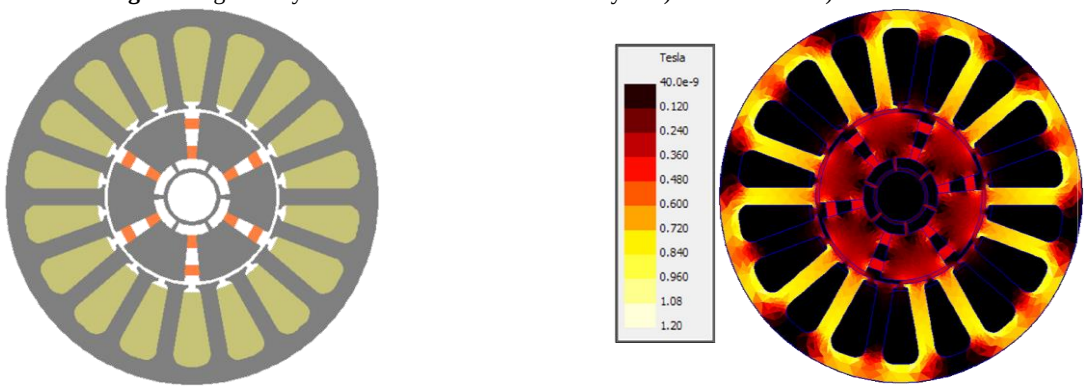

(a)

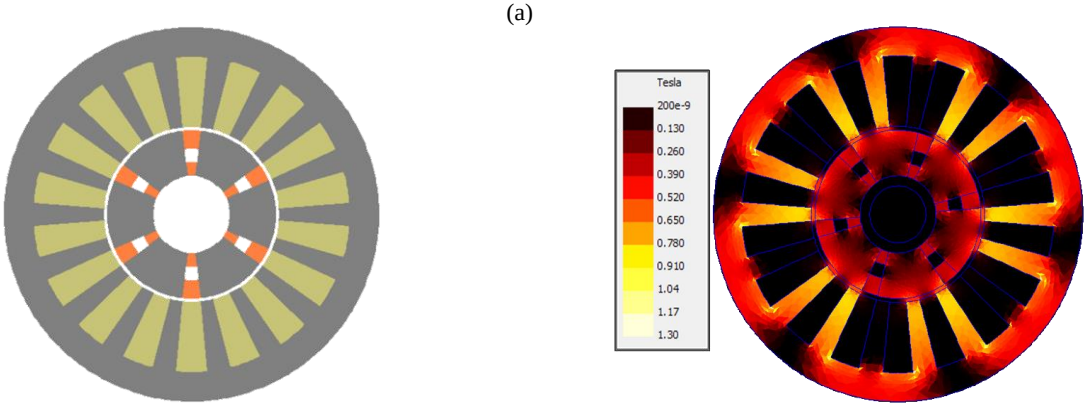

(b)

Fig. 4 2-D schematic and magnetic flux density of a) M1-design and b) M2-design.

self-inductance, mutual inductance, and phase back electromotive force are shown for M1 and M2 machines in Fig. 7 and Fig. 8, respectively. The analytical and numerical results are compared for three distinct values of iron core relative permeability. It can be seen that the results of the analytical model are in a good agreement with the results of numerical method by an error percentage of about 4.3%. A comparison of cogging torque waveforms for M1- and M2-machines are shown in Fig. 9 in which, the peak value of the cogging torque in M1 and M2 machines are 0.374548 N.m and 0.02139 N.m, respectively.

The mean values of the electromagnetic torque, the electromagnetic torque ripple, the mean values of the reluctance torque, the reluctance torque ripple, the peak back-EMF, the self-inductance, and the mutual inductance for the three values of magnetic permeability for the M1- and M-2 designs are given in Table 5. In the case of M1-design, the electromagnetic torque ripple for the iron permeability of infinite and 800, respectively, is reduced from 1.4028751 N.m to 0.562386 N.m, and for iron permeability of 200, it decreases to 0.333679. From the results of the study, it can be seen that in the M1-machine, for iron permeability values of infinity and 200, the reluctance torque ripple reduced from 1.519755 N.m to 0.3149174 N.m.

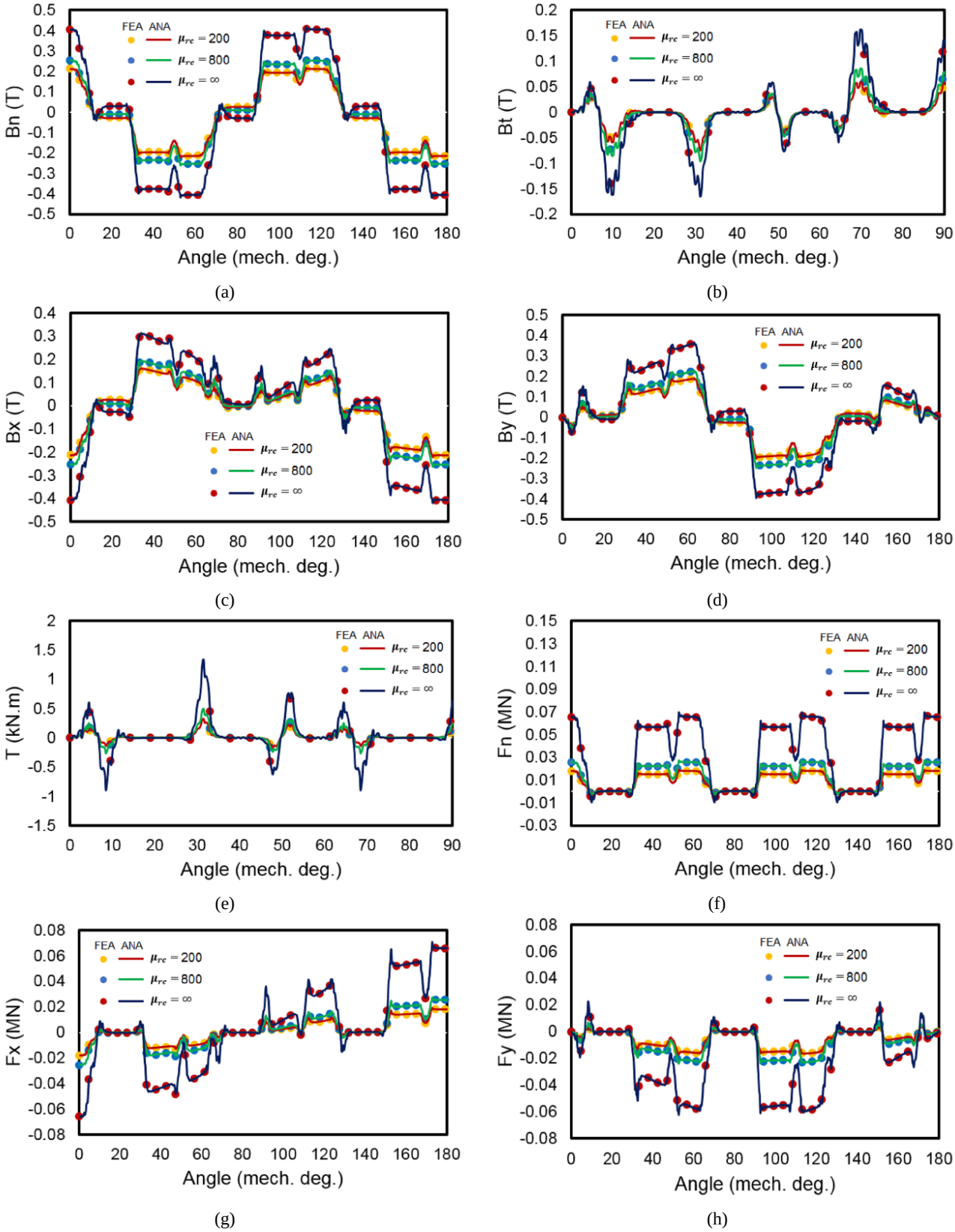

Fig. 5 On-load flux distribution of M1-design at the middle of air-gap for three distinct values of iron core relative permeability; a) radial flux density, b) tangentail flux density, c) x-component of flux density, d) y-component of flux density, e) Maxwell tensor of torque, f) Maxwell tensor of normal force, g) x-component of Maxwell tensor of force, and h) y-component of Maxwell tensor of force.

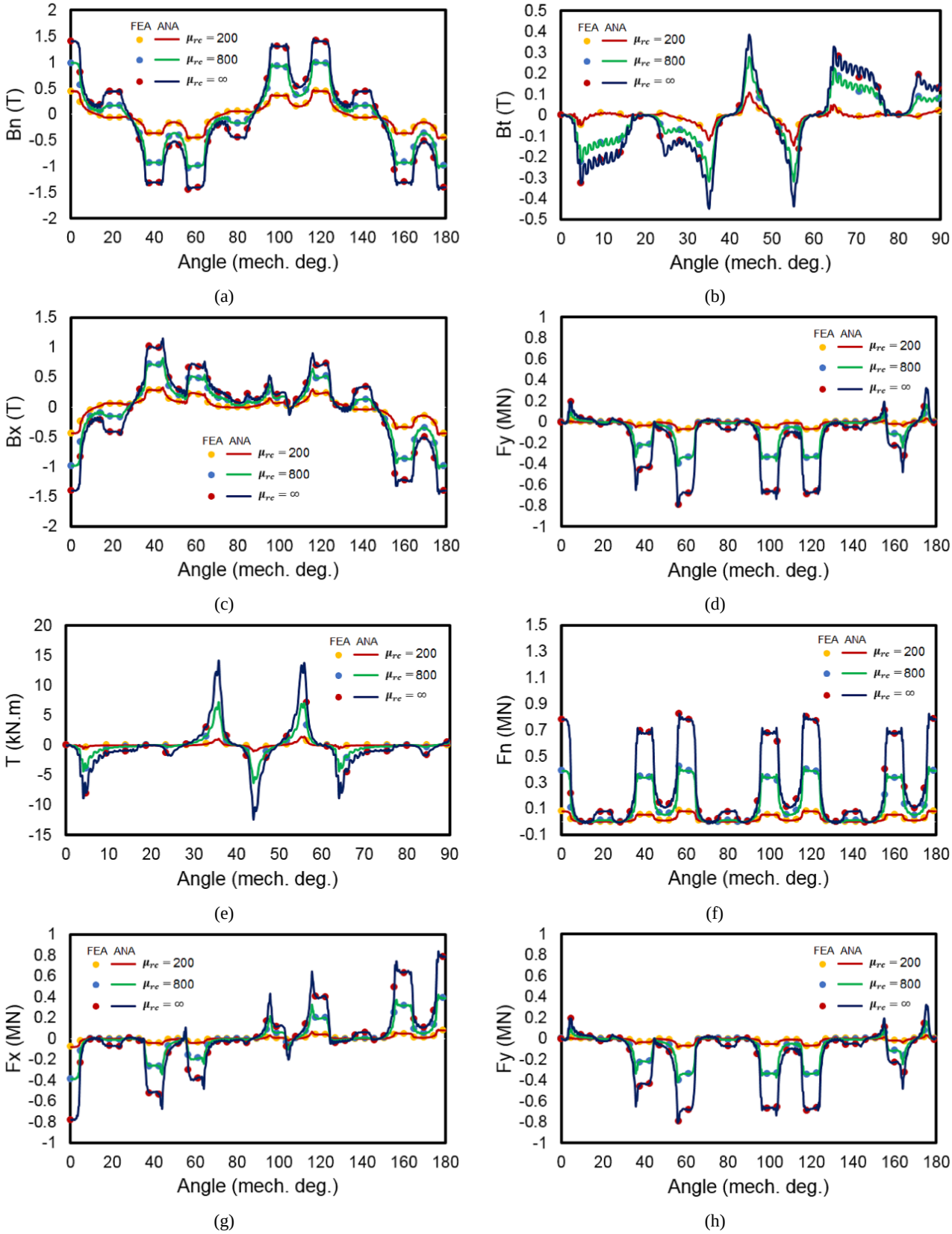

Fig. 6 On-load flux distribution of M2-design at the middle of air-gap for three distinct values of iron core relative permeability; a) radial flux density, b) tangentail flux density, c) x-component of flux density, d) y-component of flux density, e) Maxwell tensor of torque, f) Maxwell tensor of normal force, g) x-component of Maxwell tensor of force, and h) y-component of Maxwell tensor of force.

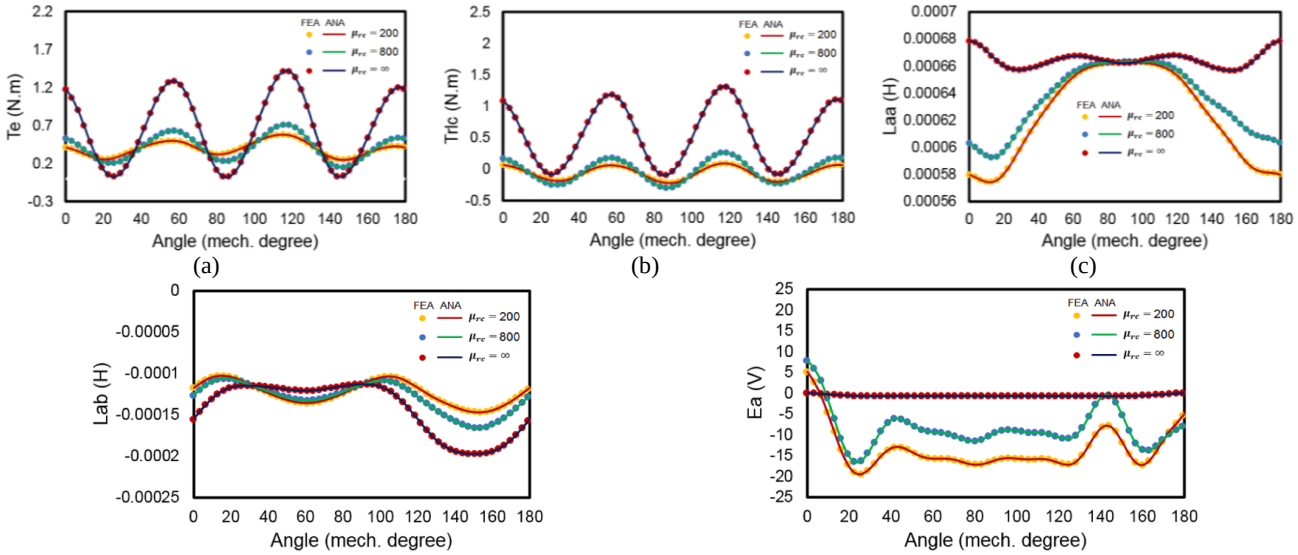

Fig. 7 Performance characteristics of M1 machine at nominal speed for three distinct values of iron core relative permeability; a) electromagnetic torque, b) reluctance torque, c) phase A self-inductance, d) phase A-phase B mutual inductance, and e) phase A back-EMF.

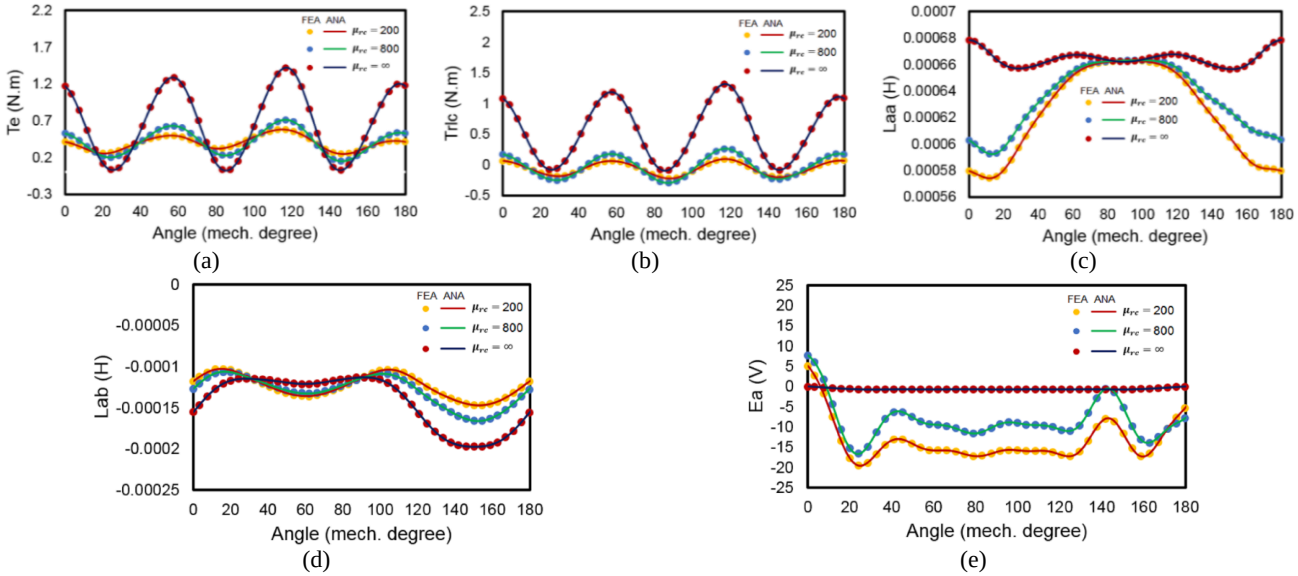

Fig. 8 Performance characteristics of M1 machine at nominal speed for three distinct values of iron core relative permeability; a) electromagnetic torque, b) reluctance torque, c) phase A self-inductance, d) phase A-phase B mutual inductance, and e) phase A back-EMF.

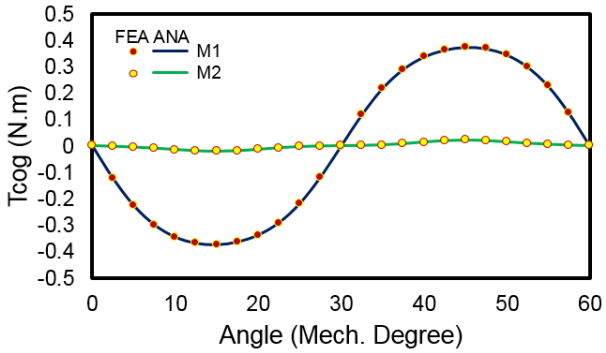

Fig. 9 A comparison of cogging torque waveforms for M1- and M2- machines.

5 Conclusion

In this paper, we present a semi-analytical method for calculating the no-load and on-load performance characteristics of magnet-segmented spoke-type machines. In addition, the effect of relative permeability of iron core on machine performance was studied, analytically and numerically. From the results of this study, it can be observed that the iron core relative permeability and magnet segmentation have a great effect on magnetic flux density distribution, radial force distribution, electromagnetic torque, reluctance torque, self/mutual inductance, and back-emf. For validation of the proposed analytical model, two different magnet-segmented spoke-type machines were investigated and numerical and analytical results were compared. Comparing these results, it can be seen that the proposed model is highly accurate.

Table 5 The studied Machine characteristics at three different soft- material relative permeability.

Machine characteristic	M2 design			M1 design		
	$\mu = \infty$	$\mu = 800$	$\mu = 200$	$\mu = \infty$	$\mu = 800$	$\mu = 200$
Average electromagnetic torque	0.657080	0.4106838	0.394950	1.42223	0.711058	0.580176
Electromagnet torque ripple	1.402875	0.562386	0.333679	1.4028751	0.562386	0.333679
Average reluctance torque	0.549567	-0.031160	-0.064578	1.3168	0.26278	0.0919834
Reluctance torque ripple	1.414424	0.559455	0.3149174	1.519755	0.559455	0.3149174
Back-emf	19.5668	16.665	0.741723	19.566	16.665	0.741723
Self-inductance	0.0006784	0.0006632	0.0006629	0.0006784	0.0006632	0.0006629
Mutual inductance	-0.0001130	-0.0001061	-0.0001027	-0.0001130	-0.0001061	-0.00010271

Appendix

Table 6 t and θ-edges interface conditions.

	***θ*-edges interface conditions (ICs)**		***t*-edges interface conditions (ICs)**
	$A_{z\Omega}\big\|_{t=t_i} = A_{z\Psi}\big\|_{t=t_j}$ and $H_{\theta\Omega}\big\|_{t=t_i} = H_{\theta\Psi}\big\|_{t=t_j}$		$A_{z\Omega}\big\|_{\theta} = A_{z\Psi}\big\|_{\theta}$ and $H_{t\Omega}\big\|_{\theta} = H_{t\Psi}\big\|_{\theta}$
$R = R_2$	$\forall\ \theta \in [\theta_l, \theta_l + \zeta]$ between Region Ω = II at t_4/Region Ψ = IV(i) at t_5 and $\forall\ \theta \in [\theta_l + \zeta, \theta_l + \zeta + \varphi]$ between Region Ω = II/Region III(i).	$\forall\ t \in [t_3, t_4]$	At $\theta = \theta_m$ between Region IV(i)/Region III(i) and $\theta = \theta_m + \psi$ between Region IV(i)/Region III(i).
$R = R_3$	$\forall\ \theta \in [\theta_m + \psi, \theta_m + \psi + \varepsilon]$ between Region Ω = V at t_7/Region Ψ = III(i) at t_6 and $\forall\ \theta \in [\theta_m, \theta_m + \psi]$ between Region Ω = VI(j)/Region Ψ = IV(i).	$\forall\ t \in [t_5, t_6]$	At $\theta = \theta_l$ between Region VI(i)/Region V(i) and $\theta = \theta_l + \zeta$ between Region VI(i)/Region V(i).
$R = R_4$	$\forall\ \theta \in [\theta_l + \zeta, \theta_l + \zeta + \varphi]$ between Region V(j) at t_8/Region VIII(k) at t_9 and $\forall\ \theta \in [\theta_l, \theta_l + \zeta]$ between Region VI(j)/Region VII(k).	$\forall\ t \in [t_7, t_8]$	At $\theta = \theta_l$ between Region VI(j)/Region V(j) and $\theta = \theta_l + \zeta$ between Region VI(j)/Region V(j).
$R = R_5$	$\forall\ \theta \in [\theta_l + \zeta, \theta_l + \zeta + \varphi]$ between Region IX at t_{11}/Region VIII(k) at t_{10} and $\forall\ \theta \in [\theta_l, \theta_l + \zeta]$ between Region IX/Region VII(k).	$\forall\ t \in [t_9, t_{10}]$	At $\theta = \theta_l$ between Region VII(k)/Region VIII(k) and at $\theta = \theta_l + \zeta$ between Region VII(k)/Region VIII(k).
$R = R_6$	$\forall\ \theta \in [\theta_j + \gamma, \theta_j + \gamma + \delta]$ between Region IX at t_{12}/Region X(l) at t_{13} and $\forall\ \theta \in [\theta_j, \theta_j + \gamma]$ between Region IX/Region XI(l).	$\forall\ t \in [t_{13}, t_{14}]$	At $\theta = \theta_j$ between Region XI(l)/Region X(l) and $\theta = \theta_j + \gamma$ between Region XI(l)/Region X(l).
$R = R_7$	$\forall\ \theta \in [\theta_j, \theta_j + \gamma/2]$ between Region XI(l) at t_{14}/Region XIII(m) at t_{15}, $\forall\ \theta \in [\theta_j + \gamma/2, \theta_j + \gamma]$ Region XI at t_{14}/Region XIV at t_{15}, $\forall\ \theta \in [\theta_i + \alpha, \theta_i + \alpha + \beta]$ between Region XII(m) at t_{15}/Region X(l) at t_{14}, $\forall\ \theta \in [\theta_i, \theta_j + \gamma]$ between Region X(l) at t_{14}/Region XIII(m) at t_{15}, $\forall\ \theta \in [\theta_j + \gamma, \theta_i + \alpha]$ between Region X(l+1) at t_{14}/Region XIII(m+1) at t_{15}, and $\forall\ \theta \in [\theta_j, \theta_j + \gamma]$ between Region XI at t_{14}/Region XIV at t_{15}.	$\forall\ t \in [t_{15}, t_{16}]$	At $\theta = \theta_i$ between Region XIII(m)/Region XII(m), at $\theta = \theta_i + \alpha/2$ between Region XIV(m)/Region XIII(m), $\theta = \theta_i + \alpha$ between Region XIV(m)/Region XII(m).
$R = R_8$	$\forall\ \theta \in [\theta_i + \alpha, \theta_i + \alpha + \beta]$ between Region XV at t_{17}/Region XII(m) at t_{16} and $\forall\ \theta \in [\theta_i, \theta_i + \alpha/2]$ between Region XV at t_{17}/Region XIII(m) at t_{16}, $\forall\ \theta \in [\theta_i + \alpha/2, \theta_i + \alpha]$ between Region XV at t_{17}/Region XIV(m) at t_{16}.		

References

[1] M. Y. Kim, Y. C. Kim, and G. T. Kim, "Design of slotless-type PMLSM for high power density using divided PM," *IEEE Transactions on Magnetics*, Vol. 40, No. 3, pp. 746–749, Mar. 2004.

[2] R. Lateb, N. Takorabet, and F. Meibody-Tabar, "Effect of magnet segmentation on the cogging torque in surface-mounted permanent-magnet motors," *IEEE Transactions on Magnetics*, Vol. 42, No. 3, pp. 442–445, Mar. 2006.

[3] A. H. Isfahani, "Analytical framework for thrust enhancement in permanent-magnet (PM) linear synchronous motors with segmented PM poles," *IEEE Transactions on Magnetics*, Vol. 46, No. 4, pp. 1116–1122, 2009.

[4] S. Duan, L. Zhou, and J. Wang, "Flux weakening mechanism of interior permanent magnet synchronous machines with segmented permanent magnets" *IEEE Transactions on Applied Superconductivity*, Vol. 24, No. 3, pp. 1–5, 2014.

[5] X. Wang, K. Yang, and Z. Pan, "Research on permanent magnet synchronous motor with segmented permanent magnet used for spindle," in *18th International Conference on Electrical Machines and Systems (ICEMS)*, pp. 200203, 2015.

[6] P. Sergarent and A. Van den Bossche, "Segmentation of magnets to reduce losses in permanent-magnet synchronous machines," *IEEE Transactions on Magnetics*, Vol. 44, No. 11, pp. 4409–4412, 2008.

[7] L. Zhu, S. Z. Jiang, Z. Q. Zhu, and C. C. Chan, "Analysis and modeling of open-circuit airgap field distributions in multi-segment and multilayer interior permanent magnet machines," in *IEEE Vehicle Power and Propulsion Conference*, pp. 1–6, 2008.

[8] A. Wang, H. Li, W. Lu, and H. Zhao, "Influence of skewed and segmented magnet rotor on IPM machine performance and ripple torque for electric traction," in *IEEE International Electric Machines and Drives Conference*, pp. 305–310, 2009.

[9] K. Yamazaki, M. Shina, Y. Kanou, M. Miwa, and J. Hagiwara, "Effect of eddy current loss reduction by segmentation of magnets in synchronous motors: Difference between interior and surface types," *IEEE Transactions on Magnetics*, Vol. 45, No. 10, pp. 4756–4759, 2009.

[10] S. M. Jang, H. J. Park, J. H. Choi, C. Han, and M. S. Choi, "Analysis on the magnetic force characteristics of segmented magnet used in large permanent-magnet wind power generator," *IEEE Transactions on Magnetics*, Vol. 49, No. 7, pp. 3981–3984, 2013.

[11] Z. Belli and M. R. Mekideche, "Optimization of magnets segmentation for eddy current losses reduction in permanent magnets electrical machines," in *Eighth International Conference and Exhibition on Ecological Vehicles and Renewable Energies (EVER)*, pp. 1–7, 2013.

[12] C. Xia, L. Guo, and H. Wa, "Modeling and analyzing of magnetic field of segmented Halbach array permanent magnet machine considering gap between segments," *IEEE Transactions on Magnetics*, Vol. 50, No. 12, pp. 1–9, 2014.

[13] M. M. J. Al-Ani and M. L. Jupp, "Switched flux permanent magnet machine with segmanted magnets," in *8th IET International Conference on Power Electronics, Machines and Drives (PEMD 2016)*, Glasgow, pp. 1–5, 2016.

[14] B. Virlan, A. Munteanu, L. Livadaru, A. Simion, and L Nacu, "Pole magnets segmentation effect on permanent magnet synchronous generators," in *International Conference on Electromechanical and Power Systems (SIELMEN)*, pp. 163–168, 2017.

[15] A. Jabbari, M. Shakeri, and A. N. Niaki, "Iron Pole shape optimization of permanent magnet synchronous motors using an integrated method," *Advances in Electrical and Computer Engineering*, Vol. 10, No. 1, pp.48–55, 2010.

[16] E. Devillers, J. L. Besnerais, T. Lubin, M. Hecquet, and J. P. Lecointe, "A review of subdomain modeling techniques in electrical machines: Performances and applications," in *XXII International Conference on Electrical Machines (ICEM)*, Lausanne, Switzerland, pp. 86–92, Sep. 2016.

[17] H. Tiegna, Y. Amara, and G. Barakat, "Overview of analytical models of permanent magnet electrical machines for analysis and design purposes," *Mathematics and Computers in Simulation*, Vol. 90, pp. 162–177, Apr. 2013.

[18] M. Curti, J. J. H. Paulides, and E. A. Lomonova, "An overview of analytical methods for magnetic field computation," in *Tenth International Conference on Ecological Vehicles and Renewable Energies (EVER)*, Grimaldi Forum, Monaco, pp. 1–7, Mar./Apr. 2015.

[19] R. L. J. Sprangers, J. J. H. Paulides, B. L. J. Gysen, J. Waarma, and E. A. Lomonova, "Semi analytical framework for synchronous reluctance motor analysis including finite soft-magnetic material permeability," *IEEE Transactions on Magnetics*, Vol. 51, No. 11, Nov. 2015.

[20] L. Roubache, K. Bougharara, and F. Dubas, "new subdomain technique for electromagnetic performances calculation in radial-flux electrical machines considering finite soft-magnetic material permeability," *IEEE Transactions on Magnetics*, Vol. 54, No. 4, pp. 1–15.

[21] L. Roubache, K. Boughrara, F. Dubas, and R. Ibtiouen, "New subdomain technique for electromagnetic performances calculation in radial-flux electrical machines considering finite soft-magnetic material permeability," *IEEE Transactions on Magnetics*, Vol. 54, No. 4, 2018.

[22] A. Jabbari, "2D analytical modeling of magnetic vector potential in surface mounted and surface inset permanent magnet machines," *Iranian Journal of Electrical and Electronic Engineering*, Vol. 13, No. 4, pp. 362–373, 2017.

[23] A. Jabbari, "Exact analytical modeling of magnetic vector potential in surface inset permanent magnet DC machines considering magnet segmentation," *Journal of Electrical Engineering*, Vol. 69, No. 1, pp. 39–45, 2018.

[24] A. Jabbari, "Analytical modeling of magnetic field distribution in multiphase H-type stator core permanent magnet flux switching machines," *Iranian Journal of Science and Technology, Transaction on Electrical Engineering*, Vol. 43, No. 1, pp. 389–401, 2019.

[25] A. Jabbari, "An analytical expression for magnet shape optimization in surface-mounted permanent magnet machines," *Mathematical and Computational Applications*, Vol. 23, No. 4, pp. 1–17, 2018.

[26] A. Jabbari, "An analytical study on iron pole shape optimization in high-speed interior permanent magnet machines," *Iranian Journal of Science and Technology, Transaction on Electrical Engineering*, Vol. 44, No. 1, pp. 169–174, 2019.

[27] F. Dubas and C. Espanet, "Analytical solution of the magnetic field in permanent-magnet motors taking into account slotting effect: No-load vector potential and flux density calculation," *IEEE Transactions on Magnetics*, Vol. 45, No. 5, pp. 2097–2109, May 2009.

[28] F. Dubas and K. Boughrara, "New scientific contribution on the 2-D subdomain technique in Cartesian coordinates: Taking into account of iron parts," *Mathematical and Computational Applications*, Vol. 22, No. 1, p. 17, Feb. 2017.

[29] K. Boughrara, R. Ibtiouen, and T. Lubin, "Analytical prediction of magnetic field in parallel double excitation and spoke-type permanentmagnet machines accounting for tooth-tips and shape of polar pieces," *IEEE Transactions on Magnetics*, Vol. 48, No. 7, pp. 2121–2137, Jul. 2012.

[30] P. Liang, F. Chai, Y. Li, and Y. Pei, "Analytical prediction of magnetic field distribution in spoke-type permanent-magnet synchronous machines accounting for bridge saturation and magnet shape," *IEEE Transactions on Industrial Electronics*, Vol. 64, No. 5, pp. 3479–3488, May 2017.

[31] M. Pourahmadi-Nakhli, A. Rahideh, and M. Mardaneh, "Analytical 2-D model of slotted brushless machines with cubic spoke-type permanent magnets," *IEEE Transactions on Energy Conversion*, Vol. 33, No. 1, pp. 373–382, 2017.

[32] A. Jabbari and F. Dubas, "A new subdomain method for performances computation in interior permanent-magnet (IPM) machines," *Iranian Journal of Electrical and Electronic Engineering*, Vol. 16, No. 1, pp. 26–38, 2020.

A. Jabbari was born in Shazand, Iran, in 1980. He received the B.Sc. degree from Iran University of Science and Technology (IUST) in 2002 and his M.Sc. and Ph.D. degrees both in Mechanical Engineering from Mazandran University in 2004 and 2009, respectively, with a focus on the design and the optimization of brushless DC permanent magnet machines for direct drive applications. He is currently an Assistant Professor with the Department of Mechanical Engineering, Arak University, Arak, Iran. Since 2014, he has been the Head of Gearless Wind Turbine Project team. His research interests include gearless wind turbine design, analytical modeling, pm machines, subdomain technique, friction stir welding, and metal forming.